Rijksuniversiteit Groningen

K.J.H. Giesbertz

Dispersion relations of carbon nanotubes

Materials Science Center
University of Groningen
Nijenborgh 4
9747 AG Groningen
+31 (0)50-363 4843
The Netherlands

Contents

1 Introduction

The first observations of carbon nanotubes were reported by Sumio Iijima in 1991 [1]. He found multi-walled carbon nanotubes by taking an electron microscope image of a carbon specimen from the negative electrode of a d.c. arc-discharge evaporator (see fig. 1). The arc-discharge evaporator is normally used for the production of the famous Buckminsterfullerene, C_{60}, but he found rod like structures. Graphitic rods were already predicted. They would exist of 2D graphite sheets which were rolled up like a sheet of paper. He found that the rods were concentric. So the rods had to be tubes of carbon atoms.

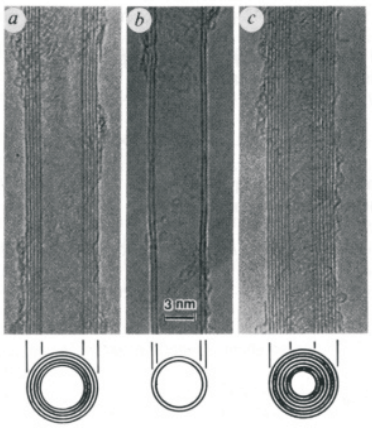

Figure 1: First electron microscope images of multi-walled carbon nanotubes published by S. Iijima.

Theoreticians were inspired by the symmetries of the structures. Band structure calculations readily showed that the tubes could be semiconducting or metallic [2, 3]. The difference between the metallic tubes and the semiconducting tubes is totally determined by the structure of the tubes, although they are made of the same element. The metallic tubes would be one-dimensional conductors which are usually unstable to Peierls distortions. However, carbon nanotubes seem to be stable to Peierls distortion well below room temperature ($\sim$ 1K) [2, 4]. It has been theoretically predicted that the metallic tubes should behave as ballistic conductors for ranges up to 10μm [5]. Ballistic conductance is indeed observed in several experiments [6, 7, 8].

These exceptional electronic properties have caused many speculations for the use of carbon nanotubes in electronics. A big problem is the processing in millions of these tubes with very high precision. Some progress has already been reported in the separation of semi-conducting tubes from metallic tubes [9] and the placement of the tubes [10, 11]. However, the processing techniques of carbon nanotubes are still not good enough to incorporate them in real electronic systems.

First, an introduction to the production of carbon nanotubes is given to get an idea of difficulties in the production of the tubes. Then the paper will focus on the band structure of the tubes. After the discovery of the tubes, two different analytical calculations of the band structure of the carbon nanotubes were published [2, 3]. Both models will be treated here. Finally, the dispersion relations will be compared with each other.

2 Carbon nanotube production

There are several techniques to produce carbon nanotubes. They can be roughly separated in three different methods. Every technique has all kinds of variations which will not be treated here.

1. The first carbon nanotubes were produced by d.c. **carbon arc-discharge evaporation** [1]. It is originally used to produce C_{60} fullerenes, but it can also be used for the production of nanotubes. It is one of the easiest methods to produce carbon nanotubes. However, the soot contains a great variety of products and catalytic particles, so the nanotubes have to be separated from them.

   Arc-discharge evaporation is executed by placing two graphite electrodes very close to each other ($\sim$ 1mm). Usually the electrodes are placed under the atmosphere of an inert gas (helium or argon) at low pressure (50 to 700 mbar). At a voltage of about 20 V, a direct current of 50 to 100 A produces a high temperature discharge between the electrodes. The discharge evaporates one of the electrodes and the soot on the other contains carbon nanotubes. Usually the anode is evaporated and the product condenses at the cathode. High yield production highly depends on the uniformity of the discharge and temperature [12].

   When pure graphite electrodes are used, the carbon nanotubes in the soot are predominantly multi-walled carbon nanotubes. When electrodes containing catalytic metal particles (Fe, Co, Ni, Y or Mo), single-walled carbon nanotubes will be formed.

   Advantage of this method is that the single-walled carbon nanotubes contain very little defects and the production process is not too expensive. A disadvantage is the short lengths of the tubes.

2. In 1995 the group of Smalley [13] reported production of carbon nanotubes by **laser ablation**. A continuous or pulsed laser is used to vaporize graphite in a oven at 1200 °C. To transport the products to the collector outside the oven, a constant flow of an inert gas is applied at a pressure of 670 mbar. The collector is cooled let single-walled carbon nanotubes condense on the collector.

   Laser ablation is very similar to arc-discharge evaporation since the environments are almost the same. If pure graphite is used, the main product will also be multi-walled carbon nanotubes. To produce single-walled carbon nanotubes a catalyst (Ni, Co, etc.) has to be added to the graphite.

   Although laser ablation resembles very much arc-discharge evaporation, laser ablation gives purer nanotubes. A disadvantage of the production of carbon nanotubes by laser ablation is that it is difficult to scale the process up. Also the production process is quite expensive, since an expensive laser is required and the laser needs a lot of power.

3. An other technique to produce carbon nanotubes is **Chemical Vapour deposition (CVD)**. It starts with a carbon source in the gas phase (methane, carbon monoxide, acetylene, etc.). Energy is transferred to the molecules by a plasma or a resistivity heated

coil to crack the molecules into reactive carbon atoms. They diffuse to a coated substrate which is heated. The carbon atoms will bind to the surface and if the right conditions are maintained, carbon nanotubes will be formed. The coating of the substrate usually consists of first row transition metals, which will act as a catalyst for the formation of single-walled carbon nanotubes.

There is a great variety of different techniques using CVD, but they all use this two step process. In general the coating is sputtered onto the substrate. After the sputtering, the catalyst is further prepared by etching or thermal annealing. This will result in particle nucleation of the catalyst from which the nanotubes will grow.

A great advantage of CVD is that the carbon nanotubes can be aligned [14] and they can be positioned with nanometer control [15]. Also this technique is very easy to scale up to large scale production. A disadvantage is that the nanotubes are predominantly multi-walled and they contain lots of defects.

3 Structure of carbon nanotubes

The most obvious way to describe a carbon nanotube is to start from a hemisphere of a C_{60} molecule. Starting from a hemisphere with a C_5 symmetry (see fig. 2(b)), one can elongate the structure by placing an additional row of five hexagons by adding equatorially a ring of ten new carbon atoms. Repeated addition of atoms gives rise to an elongated structure in the form of a tube, which can be closed by another hemisphere (see fig. 3(a)).

Another tubular structure can be obtained if one starts from a hemisphere with a C_3 symmetry (see fig. 2(c)). By adding repeatedly nine hexagons on the hemisphere, a tubular structure is created, which can be closed at the end by the same cap (see fig. 3(b)).

Since the nucleation of a carbon nanotube in general would not nucleate from a hemisphere of a C_{60} molecule, these structures will be rare. A more general description is based on the construction of the tube by wrapping a 2D graphite sheet around a cylinder. This projection can be uniquely specified by the vector $\boldsymbol{R} = n_1\boldsymbol{R}_1 + n_2\boldsymbol{R}_2$. $\boldsymbol{R}_1$ and $\boldsymbol{R}_2$ are the primitive vectors of the Bravais lattice (see fig. 4). The vector $\boldsymbol{R}$ is called the chiral vector and indicates the cells which will fall on top of each other when the sheet is rolled up. This definition enables us to label each tube by the integer pair $[n_1, n_2]$. To ensure a one to one relation between the integer pair and the tubes, the vector $\boldsymbol{R}$ is confined to a wedge of $\pm 30°$. Since the band structure will not depend on the sign of the helicity, the wedge is chosen to be between $0°$ and $+30°$. This

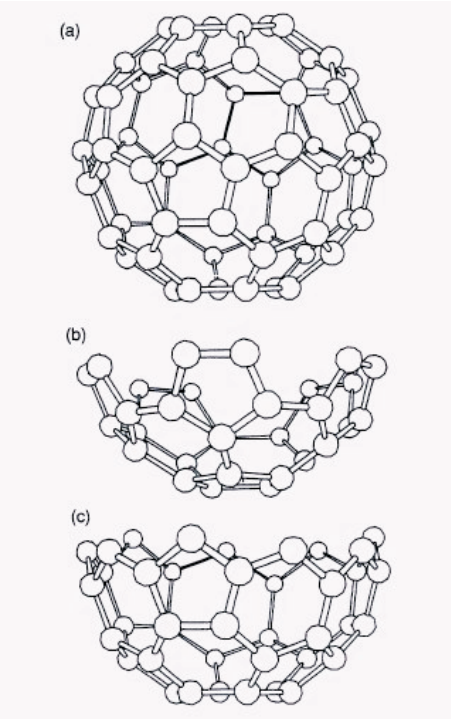

Figure 2: (a) C_{60}, (b) armchair cut and (c) zigzag cut of C_{60} to form caps for armchair and zigzag tubes.

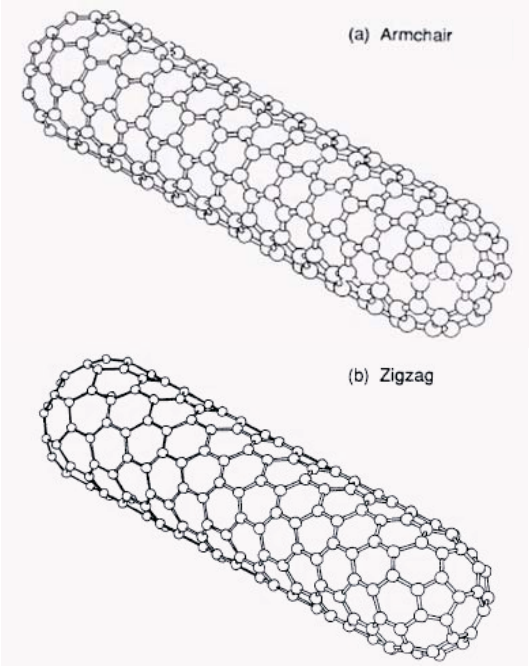

Figure 3: Atomic arrangements of carbon atoms in the (a) armchair tube and the (b) zigzag tube.

will impose the additional conditions on the integer pair $[n_1, n_2]$: $n_1 \geq n_2 \geq 0$.

In this terminology, the zigzag and armchair tubes described above are specified by [9,0] and [5,5], respectively. However, in general a nanotube is called a(n) zigzag (armchair) tube when it is described by an integer pair [n,0] ([n,n]). The armchair and zigzag carbon nanotubes are the two limiting cases of the tubes and do not have chirality, in contrast with the other tubes.

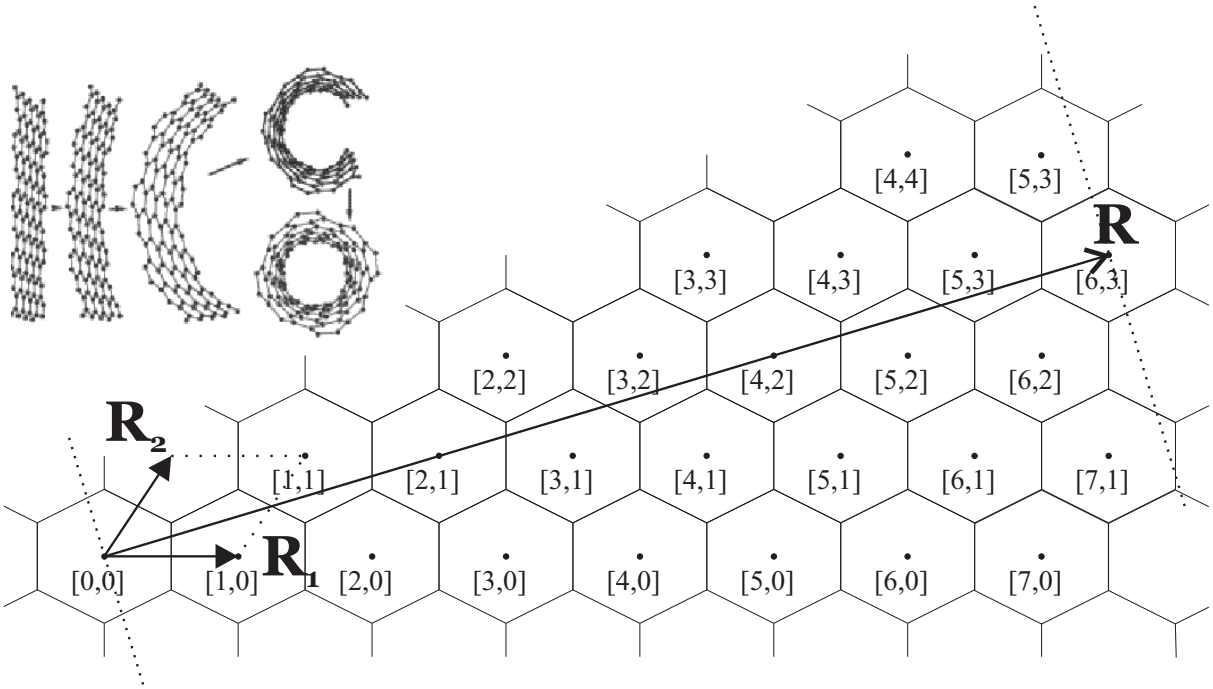

Figure 4: Irreducible wedge of the graphite lattice. $\boldsymbol{R}_1$ and $\boldsymbol{R}_2$ denote the primitive lattice vectors and the dotted lines denote the [0,0] unit cell. As an example the [6,3] chiral vector is drawn here. The dotted lines perpendicular to the [6,3] indicate the seams where the sheet is glued together.

4 Band structures

To determine the electronic properties of carbon nanotubes, the band structure has to be calculated. Two models will be presented which use a tight-binding approximation. Both models can be solved exact when only nearest neighbour interactions are taken into account. The first model relies on the electronic structure known from graphite sheets. The band structure of graphite was already calculated in 1947 by P.R. Wallace [16] by using a tight-binding approximation and taking only nearest neighbour interactions into account. Since the model for the band structure of the tubes by R. Saito et al [2, 17], uses this as a starting point for their calculations, the calculations for graphite of Wallace will also be presented here.

Another approach by C.T. White et al [3], starts from the symmetries of the tubes. These are used to construct symmetry adapted Bloch functions which will be used in a tight-binding hamiltonian. Then the model is solved analytically by taking only the nearest neighbour interactions into account.

4.1 Band structure of graphite

The band structure of graphite was already calculated by P.R. Wallace in 1947 within a tight-binding approximation [16]. The calculations relevant to a infinite 2D graphite sheet will be repeated here. A 2D graphite sheet consists of a hexagonal lattice with a spacing of 1.42Å. Carbon atoms have 4 valence electrons. Three of these form bonds by sp^2 hybridized orbitals and would not contribute to the conductivity. The z-axis is chosen to be perpendicular to the graphite sheet, so the fourth electron is considered to be in the $2p_z$ orbital.

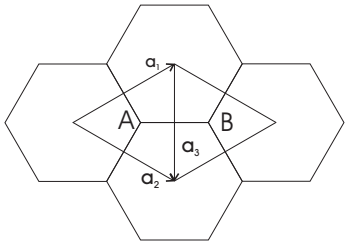

Figure 5: Real lattice of graphite. A and B are the two atoms in a unit cell. $\boldsymbol{a}_1$ and $\boldsymbol{a}_2$ are the primitive vectors of the lattice.

The hexagonal lattice of graphite contains two atoms per unit cell (fig. 5). The unit cell is spanned by the primitive translation vectors $\boldsymbol{a}_1$ and $\boldsymbol{a}_2$. The third translation vector $\boldsymbol{a}_3$ is a linear combination of the first two ($\boldsymbol{a}_3 = \boldsymbol{a}_2 - \boldsymbol{a}_1$). the length of each translation vector is $1.42 \times \sqrt{3} = 2.46\text{Å} = a$. The reciprocal vectors $\boldsymbol{b}_1$ and $\boldsymbol{b}_2$ are defined in such a way that $\boldsymbol{a}_i \cdot \boldsymbol{b}_j = 2\pi\delta_{ij}$. The length of the reciprocal lattice vectors have a magnitude $(4\pi/\sqrt{3} \times 1/a)$ $\text{Å}^{-1} = b$). The first Brillioun zone will also have a hexagonal shape, but it will be rotated 30 degrees with respect to the hexagon of the real lattice (see fig. 6).

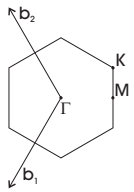

Figure 6: The reciprocal lattice of graphite. $\boldsymbol{b}_1$ and $\boldsymbol{b}_2$ are the reciprocal vectors. Γ, K and M are special symmetry points of the lattice.

A tight-binding approximation will be used to obtain a dispersion relation for graphite. Let $X(\boldsymbol{r})$ be the normalized $2p_z$ wave function. The wave function in the tight binding approximation then becomes:

$$\Psi = \alpha\phi_1 + \beta\phi_2, \tag{1}$$

where

$$\begin{cases} \phi_1 = \sum_A e^{i\boldsymbol{k}\cdot\boldsymbol{r}_A} X(\boldsymbol{r}-\boldsymbol{r}_A), \\ \phi_2 = \sum_B e^{i\boldsymbol{k}\cdot\boldsymbol{r}_B} X(\boldsymbol{r}-\boldsymbol{r}_B). \end{cases} \tag{2}$$

The first sum is taken over all lattice points A and the second over all points B. From variational principles it is known that the best approximation for the energies E is obtained by operating with the hamiltonian on the wave function Ψ and then multiplying the equation with ϕ_1 and ϕ_2 on the left, respectively. After integration two equations are obtained which can be written in matrix form as

$$\begin{pmatrix} H_{11}-ES_{11} & H_{12}-ES_{12} \\ H_{21}-ES_{21} & H_{22}-ES_{22} \end{pmatrix} \begin{pmatrix} \alpha \\ \beta \end{pmatrix} = 0, \tag{3}$$

where

$$H_{11} = \int \phi_1^* \mathcal{H} \phi_1 d\tau, \quad H_{12} = H_{21}^* = \int \phi_1^* \mathcal{H} \phi_2 d\tau, \quad H_{22} = \int \phi_2^* \mathcal{H} \phi_2 d\tau,$$
$$S_{11} = \int \phi_1^* \phi_1 d\tau, \quad S_{12} = S_{21}^* = \int \phi_1^* \phi_2 d\tau, \quad S_{22} = \int \phi_2^* \phi_2 d\tau.$$

To simplify this equation it is assumed that the overlap integral between $2p^z$ orbitals of A and B sites is zero, i.e.

$$\int X(\boldsymbol{r}-\boldsymbol{r}_A)^* X(\boldsymbol{r}-\boldsymbol{r}_A) d\tau = 0. \tag{4}$$

Since the number of sites A is equal to the number of sites B $S_{11} = S_{22} = S$. The equation only has a solution if the determinant of the matrix is zero. Together with the simplifications we obtain the following secular equation

$$\begin{vmatrix} H_{11}-ES & H_{12} \\ H_{21} & H_{22}-ES \end{vmatrix} = 0,$$

from which the following energies are found

$$E = \frac{1}{2S}\Big[H_{11}+H_{22} \pm \sqrt{(H_{11}-H_{22})^2 + 4|H_{12}|^2}\Big]. \tag{5}$$

If the overlap integrals of the $2p_z$ between the sites with the same label is neglected (which is logical since the overlap between sites A and B are already neglected) $S = N$. Also by symmetry one expects that $H_{11} = H_{22}$. The energies can then be written as

$$E = H'_{11} \pm |H'_{12}|, \quad \text{where} \quad H'_{11} = H'_{22} = \frac{1}{N}H_{11} = \frac{1}{N}H_{22}, H'_{12} = \frac{1}{N}H_{12}. \tag{6}$$

H'_{11} and H'_{12} will now be evaluated,

$$\begin{aligned} H'_{11} &= \frac{1}{N}\sum_{A,A'} e^{i\boldsymbol{k}\cdot\boldsymbol{r}_A - \boldsymbol{r}_{A'}} \int X^*(\boldsymbol{r}-\boldsymbol{r}_A)\mathcal{H}X(\boldsymbol{r}-\boldsymbol{r}_{A'})d\tau \\ &= E_0 - 2\gamma'_0\left[\cos k_y a + 2\cos\frac{\sqrt{3}k_x a}{2}\cos\frac{k_y a}{2}\right], \end{aligned} \tag{7}$$

where

$$E_0 = \int X^*(\boldsymbol{r})\mathcal{H}X(\boldsymbol{r})d\tau,$$
$$\gamma_0' = -\sum_{\boldsymbol{\rho}'}\int X^*(\boldsymbol{r}-\boldsymbol{\rho}')\mathcal{H}X(\boldsymbol{r})d\tau.$$

The sum over $\boldsymbol{\rho}'$ is taken only over the nearest neighbours among the sites A. The matrix element H_{12}' is also calculated with only the nearest neighbour interactions

$$\begin{aligned} H_{12}' &= \frac{1}{N}\sum_{A,B} e^{i\boldsymbol{k}\cdot\boldsymbol{r}_A-\boldsymbol{r}_B}\int X^*(\boldsymbol{r}-\boldsymbol{r}_A)\mathcal{H}X(\boldsymbol{r}-\boldsymbol{r}_B)d\tau \\ &= -\gamma_0\left[e^{-ik_z a\sqrt{3}} + 2e^{ik_x\frac{a}{2\sqrt{3}}}\cos\frac{k_y a}{2}\right], \end{aligned} \tag{8}$$

where

$$\gamma_0 = -\sum_{\boldsymbol{\rho}}\int X^*(\boldsymbol{r}-\boldsymbol{\rho})\mathcal{H}X(\boldsymbol{r})d\tau.$$

The sum over $\boldsymbol{\rho}$ is again taken over only the nearest neighbours. The absolute value of H_{12} then results in

$$|H_{12}|^2 = \gamma_0^2\left[1 + 4\cos^2\frac{k_y a}{2} + 4\cos\frac{k_y a}{2}\cos\frac{\sqrt{3}k_x a}{2}\right]. \tag{9}$$

The energies at varies points may now be calculated. At the symmetry points:

$$\begin{aligned} &\text{at } \Gamma: \quad E = E_0 \pm 3\gamma_0 - 6\gamma_0', \\ &\text{at } K: \quad E = E_0 + 3\gamma_0', \\ &\text{at } M: \quad E = E_0 \pm \gamma_0 + 2\gamma_0'. \end{aligned}$$

At the zone boundary there is an energy gap $\Delta E = 2|H_{12}'| = 2\gamma_0(2\cos(k_y a/2) - 1)$, which is at a maximum at the center and reduces to zero at the corners. So the energies at the corners K are degenerate.

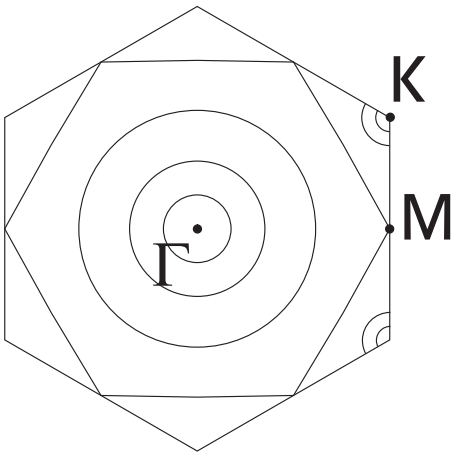

Figure 7: First Brillioun zone with contours of constant energy.

Consider now the energy contours in the first Brillioun zone (fig. 7). For energies near the Γ-point, the dispersion relation can be expanded in a Taylor series

$$E = E_0 - 3\gamma - 6\gamma_0' + \frac{a^2}{4}(\gamma_0 + 6\gamma_0')(k_x^2 + k_y^2). \qquad (10)$$

So near the Γ-point the energy contours are circular. The same expansion can be made near the corners of the zone boundary (the K-points)

$$E = E_0 + 3\gamma_0' \pm \frac{\sqrt{3}}{2}\gamma_0|\boldsymbol{k} - \boldsymbol{k}_c|a - \frac{3}{4}\gamma_0'|\boldsymbol{k} - \boldsymbol{k}_c|^2 a^2. \quad (11)$$

Another constant energy contour is the hexagon which sides are at a distance of $1/2a$ from the center of the Brillioun zone. The corners of the hexagon touch the sides of the hexagon of the Brillioun zone. This can be seen by calculating the energy for the upper or lower side of the hexagon (which will be equal to the energy in point M). By symmetry this can be extended to all sides of the hexagon (see fig. 7).

This band structure predicts that graphite would be a zero bandgap semiconductor, but it is a poor conductor. This is caused by the zero density of states near the K-points. There are no electrons to excite easily in the conduction band, so graphite is a bad conductor.

4.2 Band structure of carbon nanotubes I

Since carbon nanotubes can be described as a graphite sheet wrapped around a cylinder, the dispersion relations obtained for graphite sheets could be used as a starting point. The only additional element is an extra periodic boundary condition due to the circular symmetry of the tube. This approach was used first by R. Saito et al [2, 17]. First, the band structure of the armchair $[N_x, N_x]$ and the zigzag $[N_y, 0]$ tubes are calculated. Then the dispersion relation is extended to chiral carbon nanotubes.

First, the $[N_x, N_x]$ armchair carbon nanotube is treated. The Bravais lattice is shown in figure 8(a). Note that the x- and y-axis are defined the same as for graphite. For the armchair tubes, the cylinder axis is in the y-direction and the circumference is parallel to the x-direction. The circumference has N_x repetition units along the circumference, so boundary condition becomes:

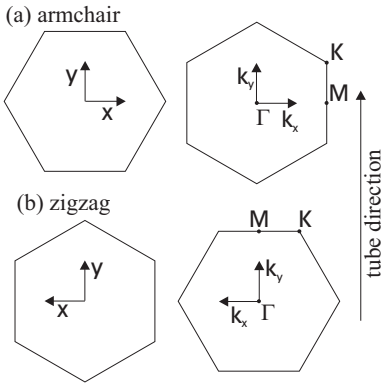

Figure 8: Bravais lattice (left) and first Brillioun zone (right) of the (a) armchair and (b) zigzag carbon nanotube.

$$N_x\sqrt{3}ak_x^q = 2\pi q \quad (q = 1, \ldots, N_x). \tag{12}$$

The dispersion relation for the armchair nanotube can be obtained by putting equation 12 in equation 9, i.e.

$$\begin{aligned} E_q^a(k) &= \pm\gamma_0 \left[1 \pm 4\cos\left(\frac{q\pi}{N_x}\right)\cos\left(\frac{ka}{2}\right) + 4\cos^2\left(\frac{ka}{2}\right)\right]^{1/2} \\ &\quad (-\pi < ka < \pi) \quad (q = 1, \ldots, N_x), \end{aligned} \tag{13}$$

where k_y is replaced by k, pointing along the tube direction. The plus and minus sign under the square-root corresponds to the unfolded and the folded energy bands, respectively. The fermi energy is set to zero.

The same can be done for the $[N_y, 0]$ zigzag nanotube which has a Bravais and reciprocal lattice shown in figure 8(b). The tube direction is now taken along the x-direction, so the periodic boundary conditions will be applied to k_y, i.e.

$$N_y a k_y^q = 2\pi q \quad (q = 1, \ldots, N_y). \tag{14}$$

Again by putting equation 14 in equation 9 and replacing k_x by k one obtains:

$$\begin{aligned} E_q^z(k) &= \pm\gamma_0 \left[1 \pm 4\cos\left(\frac{\sqrt{3}ka}{2}\right)\cos\left(\frac{q\pi}{N_y}\right) + 4\cos^2\left(\frac{q\pi}{N_y}\right)\right]^{1/2} \\ &\quad (-\frac{\pi}{\sqrt{3}} < ka < \frac{\pi}{\sqrt{3}}) \quad (q = 1, \ldots, N_y). \end{aligned} \tag{15}$$

In figure 9 the dispersion relation of the [5,5] armchair tube is plotted as E/γ_0 vs k. The thick lines indicate the double degenerate bands due to the folding. Interesting is the crossing

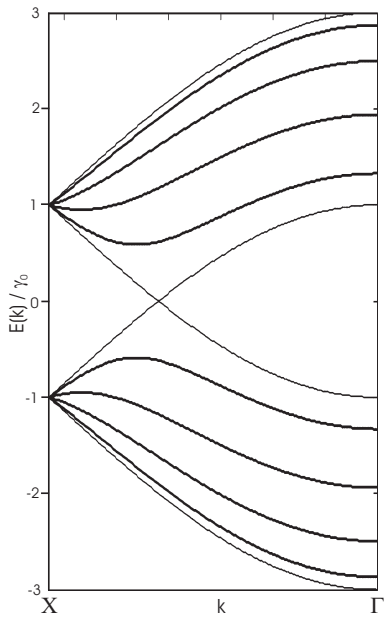

Figure 9: Energy bands for the [5,5] armchair tube. The thick lines indicate double degenerate bands.

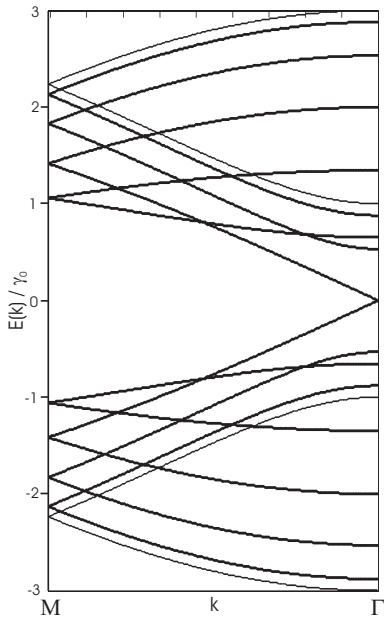

Figure 10: Energy bands for the [9,0] zigzag tube. The thick lines indicate double degenerate bands.

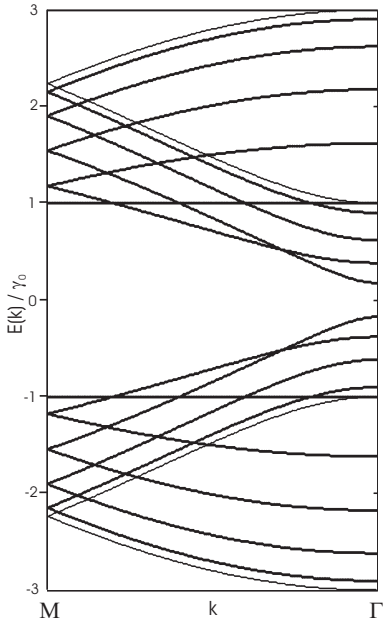

Figure 11: Energy bands for the [10,0] zigzag tube. The thick lines indicate double degenerate bands.

of the two bands at the Fermi surface at $ka = 2\pi/3$. The crossing of these bands could imply that the armchair tube is metallic. This would hold for any armchair nanotube, since for the band $q = N_x$ the energy is zero for $ka = 2\pi/3$. This point corresponds with the K-point of the graphite lattice. In graphite the density of states at this point is zero for a sheet, which makes graphite a zero bandgap semi-conductor. In contrast to graphite, calculations [18, 4, 19] and measurements [20, 21] of the density of states have shown that the density of states at the crossing is high enough for these tubes to behave as metals.

The dispersion relation for the [9,0] zigzag tube is plotted in figure 10. The energy E normalized by γ_0 is plotted vs k. Also the zigzag tube has a crossing of the energy bands, but for $k = 0$. In contrast to the armchair tubes, the bands do not cross at the Fermi surface for every nanotube. For the [10,0] zigzag tube the bands do not cross, but there is an energy gap (see fig. 11). The bands only cross at the Fermi surface when $N_y = 3/2q$ where $q \in \mathbb{N}$.

Next chiral nanotubes are considered. This is more complicated, since the periodicity can not be easy determined. In the article of Saito [2] and the book of Dresselhaus [17] it is stated that it is sufficient to impose periodic boundary conditions on the chiral vector $\boldsymbol{R}$. So the the boundary condition yields:

$$\boldsymbol{R} \cdot \boldsymbol{k} = \sqrt{3} N_x k_x a + N_y k_y a = 2\pi q. \tag{16}$$

From this this equation one can readily obtain an expression for N_x and N_y in terms of n_1 and n_2, which were defined in section 3, i.e.

$$[N_x, N_y] = \left[\frac{n_1 + n_2}{2}, \frac{n_1 - n_2}{2} \right]. \tag{17}$$

When equation 16 is put into equation 9 and k_y is replaced by k, the following dispersion relation for the chiral fibers is obtained:

$$\begin{aligned} E_q(k) &= \pm\gamma_0 \left[1 \pm 4\cos\left(\frac{q\pi}{N_x} - \frac{N_y}{N_x}\frac{ka}{2}\right)\cos\left(\frac{ka}{2}\right) + 4\cos^2\left(\frac{ka}{2}\right)\right]^{1/2} \\ & (-\pi < ka < \pi) \quad (q = 1, \ldots, N_x). \end{aligned} \tag{18}$$

From this equation follows that if a tube is to be metallic, N_y has to be 3 times a half integer for any N_x [2]. When this condition is rewritten in terms of n_1 and n_2, one obtains:

$$n_1 - n_2 = 3q \quad \text{with} \quad q \in \mathbb{Z}, \tag{19}$$

or another way of writing used by Saito and Dresselhaus:

$$2n_1 + n_2 = 3q \quad \text{with} \quad q \in \mathbb{Z}. \tag{20}$$

as condition for the tubes to be metallic. Since the integers q in the equations do not have to be the same, they are equivalent.

An other way to predict the metallic behaviour, is to look what the periodic boundary condition does to the reciprocal space [22]. When the allowed k vectors are drawn in the first Brillioun zone one readily sees if the tube is a conductor. If the allowed k vectors intersect the K-points, the tube will be metallic (and vice versa). In figure 12, this is done for the [6,0] zigzag tube. The region $M - \Gamma - M$ is divided into 6 parts. The allowed k vectors intersect the K-points, so the [6,0] behaves metallic, which is in agreement with equation 19.

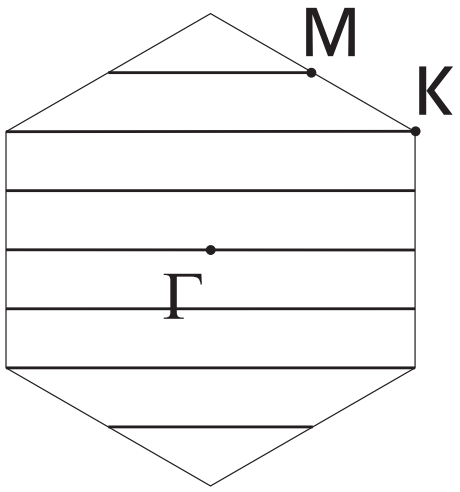

Figure 12: The first Brillioun zone of graphite. The lines indicate the allowed k vectors for the [6,0] tube.

4.3 Band structure of carbon nanotubes II

C.T. White et al [3] use a different approach. They start by describing the symmetries of the tubes first. From these symmetries they construct symmetry adapted Bloch functions which they use to solve the band structure within the tight-binding approximation. An analytical solution is obtained by taking only the nearest neighbour interactions into account.

The symmetries of the tube can be derived by considering the mapping of the 2D graphite sheet onto a cylinder of radius $|\boldsymbol{R}|/2\pi$. The two carbon atoms in the unit cell $[0,0]$ are located at $\boldsymbol{d} \equiv (\boldsymbol{R}_1 + \boldsymbol{R}_2)/3$ from each other. The first atom can be mapped onto an arbitrary point of the cylinder. The second atom is located at a point determined by $\boldsymbol{R}$ and $\boldsymbol{d}$. This point is found by a rotation of $2\pi(\boldsymbol{d}\cdot\boldsymbol{R})/|\boldsymbol{R}|^2$ radians around the cylinder axis together with a translation of $|\boldsymbol{d}\times\boldsymbol{R}|/|\boldsymbol{R}|$ parallel to the cylinder.

The largest common devisor of n_1 and n_2 will define a C_N axis that coincides with the cylinder axis. The position of the first two atoms can then be used to located $2(N-1)$ additional atoms by rotating $(N-1)$ times $2\pi/N$ radians. These $2N$ specify all the separate helical motives on the cylinder surface. The atoms occupy an area on the cylinder surface of $A_M = N|\boldsymbol{R}_1 \times \boldsymbol{R}_2|$. To generate the rest of the helices the corresponding screw operation $S(h,\alpha)$ has to be determined. There must exist a lattice vector $\boldsymbol{H} = p_1\boldsymbol{R}_1 + p_2\boldsymbol{R}_2$, where p_1 and p_2 are integers such that $h = |\boldsymbol{H}\times\boldsymbol{R}|/|\boldsymbol{R}|$ and $\alpha = 2\pi(\boldsymbol{H}\cdot\boldsymbol{R})/|\boldsymbol{R}|^2$. Since h is the distance parallel to the cylinder axis to the next cell, the area A_M should be equal to $h|\boldsymbol{R}| = |\boldsymbol{H}\times\boldsymbol{R}|$. This results in the condition $|\boldsymbol{H}\times\boldsymbol{R}| = N|\boldsymbol{R}_1\times\boldsymbol{R}_2|$ or in terms of the coefficients

$$p_2 n_1 - p_1 n_2 = \pm N. \tag{21}$$

This is the only constraint on $\boldsymbol{H}$ and so on $S(h,\alpha)$. One can readily see that an infinite number of combinations satisfy equation 21. If a set of integers $\{p_1, p_2\}$ satisfy equation 21, then also will the sets $\{p_1 \pm n_1, p_2 \pm n_1 2\}$ and $\{-p_1, -p_2\}$. To get a unique pair of integers the plus sign in equation 21 is chosen and the additional condition $p_1 \geq 0$. Together with the restriction on $\boldsymbol{R}$ $(n_1 \geq n_2 \geq 0)$ and taking the solution that yield the minimal value of $|\boldsymbol{H}|$, the set (p_1, p_2) will be unique. These choices restrict $S(h,\alpha)$ to the right-handed screw operations along the cylinder axis.

The rotational and helical symmetries can be used to describe the electronic properties of the tube. To solve the electronic structure a tight-binding hamiltonian will be used for tube lengths going to infinity. Every unit cell can be denoted by the integer pair (m,l), in which l denotes the number of times that the rotation operator C_N is used and m denotes how many $S(h,\alpha)$ is used. A unit cell located in the plane at $\boldsymbol{r} = q_1\boldsymbol{R}_1 + q_2\boldsymbol{R}_2$ will correspond to a cell labelled by (m,l). Using the definitions of $\boldsymbol{R}$ and $\boldsymbol{H}$ and equation 21 one obtains the following expressions for m and l:

$$m = (q_2 n_1 - q_1 n_2)/N \quad \text{and} \quad l = q_1 p_2 - q_2 p_1. \tag{22}$$

Assume that each atom is described by j atomic-centered basis functions, so every unit cell contains $2j$ basis functions. Let $|m,l>$ denote a vector with 2j elements containing the $2j$ basis functions of the two carbon atoms in the unit cell. Because $S(h,\alpha)$ and C_N commute, symmetry adapted generalized Bloch sums can be constructed:

$$|\kappa,n>=\lim_{M\to\infty}\frac{1}{\sqrt{2NM}}\sum_{m=-M}^{M}\sum_{l=0}^{N-1}e^{i\kappa m}e^{2\pi inl/N}|m,l>\,. \tag{23}$$

These Bloch sums have the properties that $C_N|\kappa,n>=e^{-2\pi in/N}|\kappa,n>$ with $n=0,...,N-1$ and $S(h,\alpha)|\kappa,n>=e^{-i\kappa}|\kappa,n>$ with $-\pi<\kappa\leq\pi$. The matrix elements $<\kappa',n'|\mathcal{H}|\kappa,n>$ vanish, unless $n=n'$ and $\kappa=\kappa'$. So the eigen energies of the system will be given by:

$$\epsilon_n(\kappa)=\sum_{m=-\infty}^{\infty}\sum_{l=0}^{N-1}e^{i\kappa m}e^{2\pi inl/N}<0,0|\mathcal{H}|m,l>\,. \tag{24}$$

This expression for the energies reduces the sizes of the matrices that have to be diagonalized. If all the valence s and p orbitals are used the problem is reduced to the diagonalization of a 8×8 matrix. From basic chemistry one can guess that the highest occupied and lowest unoccupied valence bands should be primarily formed by the p orbitals perpendicular to the cylinder surface. First principles local density functional calculations approve these assumptions [2, 4]. If this assumption is used, the matrix reduces even further to a 2×2 matrix. Diagonalizing this 2×2 matrix yields:

$$\begin{aligned}\epsilon_n(\kappa) &= \pm\gamma_0\Bigg[3+2\cos\left(\frac{n_1\kappa-2\pi np_1}{N}\right)+2\cos\left(\frac{n_2\kappa-2\pi np_2}{N}\right)\\ &\quad +2\cos\left(\frac{[n_1+n_2]\kappa-2\pi n[p_1+p_2]}{N}\right)\Bigg]^{1/2},\end{aligned} \tag{25}$$

where p_1 and p_2 are given by equation 21, $n=0,\ldots,N-1$ and $-\pi<\kappa<\pi$. To obtain this result, only the nearest neighbour interaction within a cell an the nearest neighbour interaction with the four neighbouring cells are taken into account. Also the small differences in the matrix element γ_0, that arise due to different bond directions on the tube surface, are neglected. To find the four neighbouring cells of the (0,0) cell, equation 22 can be used. The neighbouring cells are located at $S^{\mp n_1/N}C_N^{\pm p_1}$ and $S^{\pm n_2/N}C_N^{\mp p_2}$.

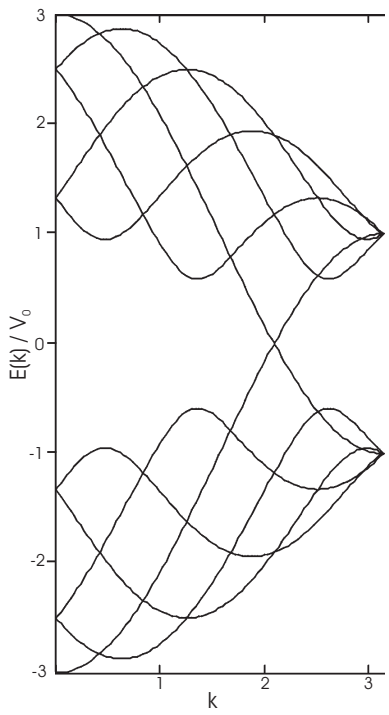

Figure 13: Energy bands for the [5,5] armchair tube.

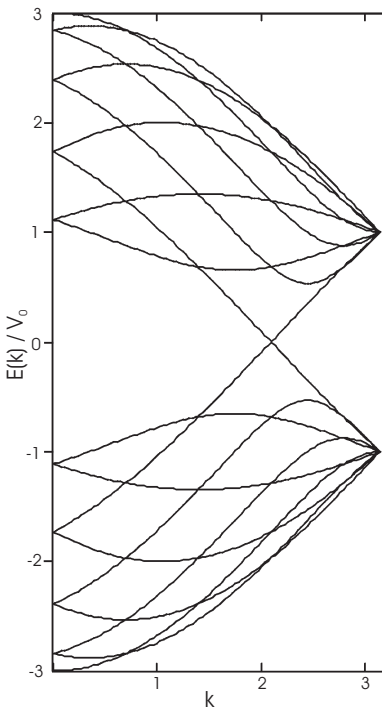

Figure 14: Energy bands for the [9,0] zigzag tube.

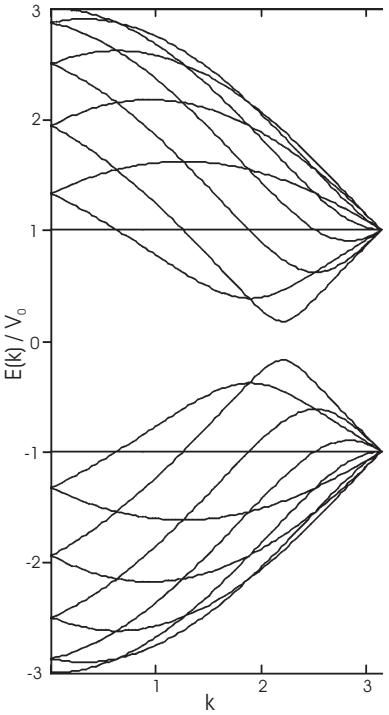

Figure 15: Energy bands for the [10,0] zigzag tube.

In the figures 13, 14 and 15 the dispersion relation for the same tubes as in the previous section are plotted. The bands for the [5,5] armchair tube cross at $\kappa = 2\pi/3$, which is similar to the band structure given by equation 18. The band structure of the [9,0] zigzag tube has a crossing of the energy bands also at $\kappa = 2\pi/3$, this in contrast to the dispersion relations given by equation 15. Also for the [10,0] zigzag tube, the bandgap is shifted from 0 to $2\pi/3$.

Despite these differences, both dispersion relations give the same condition for the tubes to be metallic: $n_1 - n_2 = 3q$ where q is an integer (eq.19).

Also the dispersion relations for the chiral tubes will differ. One can readily see this by considering the number of bands predicted by each model. As an example, consider the [n,1] tube. The first model predicts $N_x = (n_1 + n_2) = n + 1$ bands, but the second model gives only one band, since the largest common devisor is 1. In the discussion I will try to indicate what causes these discrepancies and show that these dispersion relations do not differ that much.

5 Discussion

The dispersion relations obtained by the methods in the previous section are not the same. As an example, the dispersion relation of Dresselhaus' model for the zigzag tubes, given by equation 15, is written in a similar form as the dispersion relation of White's model (eq. 25):

$$E_q^z(k) = \pm\gamma_0 \left[3 + 2\cos\left(\frac{\sqrt{3}ka}{2} + \frac{q\pi}{N_y}\right) + 2\cos\left(\frac{\sqrt{3}ka}{2} - \frac{q\pi}{N_y}\right) + 2\cos\left(\frac{2\pi q}{N_y}\right) \right]^{1/2}. \quad (26)$$

What causes these differences? To answer this question the models have to be treated more carefully than they were presented in their publications.

Let us first take a closer look at Dresselhaus' model. When the dispersion relation for chiral tubes (eq. 18) is taken into consideration, one notices that for armchair tubes it will converge to the dispersion relation 13, but it does not look to converge to equation 15 since it has a totally different structure. The dispersion relation for the chiral tubes with the parameters for the zigzag tube ($N_x = N_y = n/2$) is as follows:

$$E_q(k) = \pm\gamma_0 \left[1 + 4\cos\left(\frac{q\pi}{N_x} - \frac{ka}{2}\right)\cos\left(\frac{ka}{2}\right) + 4\cos\left(\frac{ka}{2}\right) \right]^{1/2}. \quad (27)$$

A remarkable feature of this equation is that the energy becomes zero for $ka = 2\pi/3$ instead of $ka = 0$. The problem is that k is not the vector parallel to the tube axis, but is in fact k_y. Equation 16 can be used to obtain an expression for k_x:

$$k_x = \frac{2\pi q}{\sqrt{3}N_x} - \frac{N_y k_y}{\sqrt{3}N_x}, \quad (28)$$

where ka is replaced by k and this will also be done fore the components. Since both components are known, the k-vector can be decomposed in a vector parallel to the tube and a vector perpendicular to the tube, i.e.

$$k_\parallel = \frac{\boldsymbol{R}\cdot\boldsymbol{k}}{|\boldsymbol{R}|} = \frac{2\pi q}{|\boldsymbol{R}|} \quad \text{and} \quad |k_\perp| = \frac{|\boldsymbol{R}\times\boldsymbol{k}|}{|\boldsymbol{R}|} = |\frac{2\pi q}{\sqrt{3}|\boldsymbol{R}|}\frac{N_y}{N_x} - \frac{|\boldsymbol{R}|}{\sqrt{3}N_x}k_y|. \quad (29)$$

Equation 29 can be used to express k_y in terms of $k_\perp$, i.e.

$$k_y = \frac{2\pi q N_y}{|\boldsymbol{R}|^2} \pm \frac{\sqrt{3}N_x}{|\boldsymbol{R}|}k_\perp. \quad (30)$$

A problem is that the sign in equation 30 is not determined, since only the length of $k_\perp$ is determined in equation 29. Since the dispersion relation is symmetric for $k_\perp$ ($E(k_\perp) = E(-k_\perp)$), the choice does not matter.

If the expression for k_y (eq. 30) is put into equation 18 one obtains a general expression. This is very big equation which is not very instructive to denote here. However, it is nice to consider one special case, i.e. the zigzag tube. For the zigzag tube ($[n, 0]$), one has $N_x = N_y = n/2$ and $|\boldsymbol{R}| = n = 2N_x$. When these parameters are used and equation 18 is rewritten in terms of $k_\perp$ and n, one obtains the dispersion relation given in equation 15. This is a nice result, since it has been shown that the model is at least consistent with itself.

Since the directions of the k-vector in the model of Dresselhaus causes so much trouble, this might also cause the discrepancies between the models. The label n for the energy bands is determined by rotation symmetry, so this would indicate that it is perpendicular to the tube axis. The variable κ is along the screw symmetry, on the contrary. To fix this problem the screw symmetry can be considered as a translation parallel to the tube axis, $\boldsymbol{T} = p_1\boldsymbol{R}_1 + p_2\boldsymbol{R}_2$, and a rotation around the tube. It is sufficient to calculate the translation, since the rotation is given by equation 22.

The translation is determined by p_1 and p_2, so two equations are needed to determine the translation. Equation 21 is obtained for the translation component of the screw vector $\boldsymbol{H}$ and independent of the rotation. So the translation vector $\boldsymbol{T}$ has to satisfy equation 21 and the additional condition that it has to be parallel to the chiral vector $\boldsymbol{R}$. The last condition can be found in terms of p_1 and p_2 by finding a vector perpendicular to $\boldsymbol{R}$:

$$\boldsymbol{R}_\perp \equiv 2\boldsymbol{R} \times \boldsymbol{e}_z = -(2n_2 + n_1)\boldsymbol{a}_1 + (2n_1 + n_2)\boldsymbol{a}_2. \tag{31}$$

If the screw vector is chosen along $\boldsymbol{R}_\perp$, p_1 and p_2 have to satisfy the following condition:

$$\frac{p_1}{p_2} = -\frac{2n_2 - n_1}{2n_1 + n_2}. \tag{32}$$

As an example let us consider the zigzag tubes. Equation 21 gives us $p_2 = 1$ and p_1 is undetermined. If $\boldsymbol{H}$ is chosen to be perpendicular to $\boldsymbol{R}$, $p_1 = -1/2$. The following dispersion relation is then obtained:

$$\begin{aligned} \epsilon_n(\kappa) &= \pm\gamma_0 \left[3 + 2\cos\left(\kappa + \frac{\pi n}{N}\right) + 2\cos\left(\frac{2\pi n}{N}\right) + 2\cos\left(\kappa - \frac{\pi n}{N}\right)\right]^{1/2} \\ &= \pm\gamma_0 \left[1 + 4\cos(\kappa)\cos\left(\frac{\pi n}{N}\right) + 4\cos^2\left(\frac{\pi n}{N}\right)\right]^{1/2}. \end{aligned} \tag{33}$$

This is the same dispersion relation given by Drsselhaus' model. It should be the same, since both models use a tight-binding approximation with only the nearest neighbour interactions. Note that the prediction of the width of the bandgap will not change, since the k-vector has a one-to-one relation with its components.

The only real discrepancy between the models is the number of bands they predict. The difference is that White's model uses the symmetries to determine the bands and Dresselhaus' model neglects them. So from this point of view, White's model is preferable.

6 Bibliography

References

[1] S. Iijima; *Nature*, **354** (1991) 56

[2] R. Saito, M. Fujita, G. Dresselhaus, M.S. Dresselhaus; *Phys. Rev. B*, **46** (1992) 1804

[3] C.T. White, D.H. Robertson, J.W. Mintmire; *Phys. Rev. B*, **47** (1993) 5485

[4] J.W. Mintmire, B.I. Dunlap, C.T. White; *Phys. Rev. Let.*, **68** (1992) 631

[5] C.T. White, T.N. Todorov; *Nature*, **393** (1998) 240

[6] S. Frank, P. Poncharal, Z.L. Wang, W.A. de Heer; *Science*, **280** (1998) 1744

[7] S. Sanvito, Y. Kwon, D. Tománek, C.J. Lambert; *Phys. Rev. Let.*, **84** (2000) 1974

[8] A. Urbina, I. Echeverría, A. Pérez-Garrido, A. Díaz-Sánchez, J. Abellán; *Phys. Rev. Let.*, **90** (2003) 106603

[9] P.G. Collins, M.S. Arnold, P. Avouris; *Science*, **292** (2001) 706

[10] J. Kong, H.T. Soh, A.M. Cassell, C.F. Quate, H. Dai; *Nature*, **395** (1998) 878

[11] S.G. Rao, L. Huang, W. Setyawan, S. Hong; *Nature*, **425** (2003) 36

[12] T. W. Ebbesen, P. M. Ajayan; *Nature*, **358** (1992) 220

[13] T. Guo, P. Nikolaev, A. Thess, D.T. Colbert, R.E. Smalley; *Chem. Phys. Let.*, **243** (1995) 49

[14] Z.F. Ren, Z.P. Huang, J.W. Xu, J.H. Wang, P. Bush, M.P. Siegel, P.N. Provencio; *Science (Washington, D.C.)*, **282** (1998) 1105

[15] Z.F. Ren, Z.P. Huang, D.Z. Wang, J.G. Wen, J.W. Xu, J.H. Wang, L.E. Calvet, J. Chen, J.F. Klemic, M.A. Reed; *Appl. Phys. Let.* **75** (1999) 1086

[16] P.R. Wallace; *Phys. Rev.*, **71** (1947) 622

[17] M.S. Dresselhaus, G. Dresselhaus, P.C. Eklund; *Science of Fullerenes and Carbon Nanotubes* (Academic Press, San Diego) 1996

[18] R. Saito, M. Fujita, G. Dresselhaus, M.S. Dresselhaus; *Appl. Phys. Let.*, **60** (1992) 2204

[19] J.W. Mintmire, C.T. White; *Phys. Rev. Let.*, **81** (1998) 2506

[20] J.W.G. Wildöer, L.C. Venema, A.G. Rinzler, R.E. Smalley, C. Dekker; *Nature*, **391** (1998) 59

[21] T.W. Odom, J. Huang, P. Kim, C.M. Lieber; *Nature*, **391** (1998) 62

[22] N. Hamada, S. Sawada, A. Oshiyama; *Phys. Rev. Let.*, **68** (1992) 1579